

Ensemble Flood Forecasting Using Transposition of NWP Rainfall Fields Considering Orographic Rainfall

Wansik YU⁽¹⁾, Eiichi NAKAKITA, Sunmin KIM⁽²⁾, and Kosei YAMAGUCHI

(1) Graduate School of Engineering, Kyoto University

(2) Department of Civil and Earth Resources Engineering, Kyoto University

Synopsis

The use of meteorological ensembles to produce sets of hydrological predictions has increased the ability to issue flood warnings. However, the spatial scale of a hydrological domain is still much finer than that of a meteorological model, and Numerical Weather Prediction (NWP) models have challenges with misplacement. This study assesses the transposition method with consideration of a spatial shift of ensemble NWP rainfall fields with the separation of orographic and non-orographic rainfall, in order to improve the accuracy improvement of the ensemble flood forecasting. The analysis shows that transposition of ensemble NWP rainfall fields improved the accuracy of the mean value and best value compared with original ensemble flood forecasting.

Keywords: Ensemble NWP rainfall, flood forecasting, transposition, accuracy improvement

1. INTRODUCTION

Flood forecasting is an important technique to reduce damages from flood disasters. The accuracy of weather forecasts has improved over the years, due to advances in NWP techniques and increased computing power. Thus, it is now possible to generate high-resolution rainfall forecasts at the catchment scale and to integrate quantitative precipitation forecasting (QPF) into flood forecasting systems with extended lead time (Demeritt et al., 2007; Cuo et al., 2011).

At the same time, one of the rising research themes in the flood forecasting area is the development of ensemble prediction systems (EPSs). EPSs have been used to account for uncertainties and have resulted in better quantitative predictability for the same location and time.

Several authors have utilized and investigated EPS, and found that ensembles increase forecast accuracy and allow for skillful predictions with lead time (Buizza et al., 1999; Xuan et al., 2009; Palmer and Buizza, 2007; Roulin and Vannitsem, 2005; Yu et al., 2013a).

However, in many cases, the potential of forecasting with EPS is described alongside more cautious approaches to the considerable variability and uncertainty in operational flood forecasting.

First, the time/spatial scale of the hydrological model is still much finer than that of the meteorological model. Although the NWP-based QPF can generally catch the rainfall pattern, the uncertainties of rainfall to the catchment scale were always significant. Schaake et al. (2004) analyzed the statistical properties of the prediction outcomes from the US National Centers for Environmental

Prediction (NCEP) during 1997 and 1999 over the continental US. They stated that ensemble forecasts contain biases that must be removed before they are used as an input for hydrologic models.

Second, NWP models have challenges with misplacement of the forecasting rainband, which means that the intensity and shape of the forecasted storm cell may be correct, but the location of the storm cell is wrong. Ebert and McBride (2000) stated that QPF quality needs to be improved, in order to provide reliable hydrologic prediction, and that errors in location misplacement, timing, and intensity hampered the direct application of QPF from the NWP into hydrologic prediction models.

Given the current issue and problem with EPSs with NWP models, a proper pre-processing dealt with spatial misplacement of rainfall distributions should be considered carefully, in order to use EPSs effectively in flood forecasting systems on a small catchment scale. Yu et al. (2013b) have utilized and investigated this ensemble NWP rainfall forecast for real-time flood forecasting, and proposed the spatial shift (hereafter, transposition) of ensemble rain distributions to improve the accuracy of flood forecasting. However, in case of the transposition of rain distributions in mountainous areas, the problem arises that the orographic rain patterns also move to non-mountain area with the transposition scheme. As a result, it results in a great loss of physical meaning of orographic rainfall.

The aim of this research is to address the uncertainties in ensemble hydrological forecasting driven by ensemble NWP rainfall and to explore an accuracy improvement of flood forecasting by transposition of ensemble NWP rainfall fields with the separation of orographic and non-orographic rainfall. For these objectives, ensemble NWP rainfalls are separated into orographic and non-orographic rain fields by solving physically-based equations, including additional atmospheric variables, such as vertical wind velocity. And then, the non-orographic rainfall fields are examined by transposition method to correct the misplaced spatial position. Lastly, Ensemble NWP rainfall fields are calculated by combining the transposition results of non-orographic rain fields with the orographic rainfall fields. We also apply into rising limb and

peak discharge periods to confirm an accuracy improvement of flood forecasting skill. The flood forecasting results of proposed method on ensemble NWP rainfall prediction was compared with the results of original ensemble flood forecasting, which was carried out by Yu et al. (2013b) using the Typhoon Talas event of 2011.

2. METHODOLOGY

2.1 Physically-based method for orographic rainfall

Tatehira (1976) proposed a physically-based method for calculating orographic and non-orographic rainfall fields from observed radar rainfall measurements. In this method, the orographic effect is calculated based on the seeder-feeder mechanism. The precipitation droplets or ice particles fall from an upper-level precipitating cloud (seeder) and collect cloud water as they pass through a lower-level orographic stratus cloud (feeder) by collision and coalescence, thus producing greater precipitation on the mountainous area under the cap cloud than on the nearby flat regions.

The strong rain-bands stagnated near the mountain top (orographic rainfall) are estimated using additional atmospheric variables. The flux of cloud water content L (g/m^3) in rising air parcel along with a wind is calculated by equation (1).

$$\frac{dL}{dt} = -cL - a(L - L_c) + WG - WL \left(\frac{\partial \ln \rho_v}{\partial z} \right) \quad (1)$$

where ρ_v is the density of water vapor (g/m^3), c is the ratio of cloud drops captured by seeder hydrometeors of an upper-level, a is the ratio of precipitation particles to cloud drops, L_c is the threshold amount of water content before conversion into precipitation (g/m^3) and G is the amount of saturated water vapor ρ_s increased by a rising saturated air parcel (g/m^4) (i.e. $-\rho_s/dz$). Finally, W is the vertical wind velocity (m/s), which is estimated by an inner product of horizontal wind and gradient of topographic height using DEM.

These atmospheric variables (Air temperature, horizontal wind, relative humidity) are estimated by

the use of Grid Point Value (GPV) data from Japan Meteorological Agency (JMA), and are solved in the seven layers at heights of 200, 400, 1000, 2000, 3000, 4000, and 5000 m in the σ -vertical coordinate system using the method of Nakakita et al. (1996). In equation (1), the first and second terms on the right-hand side are related with that the amount of water content is decreased. The third term shows the water vapor condensing as the air parcel ascends with a unit distance. The last term expresses the influence of atmospheric compressibility, and can be ignored because the order of this term is less than other terms. The amounts of cloud water content in an inflow and outflow mesh (L_{in} and L_{out}) can be calculated by the integral of equation (1) with respect to time t .

$$L_{out} = \frac{WG + aL_c}{c+a} + \left(L_{in} - \frac{WG + aL_c}{c+a} \right) e^{-(c+a)\Delta t} \quad (2)$$

In this study, the ensemble NWP rainfall RNWP is interpreted to be the summation of orographic rainfall R_o and non-orographic rainfall R_n (Equation (3)). Nakakita and Terazono (2008) suggested the equation (4) for orographic rainfall intensity R_o (mm/h) and assumed that the ratio c of cloud drops captured by raindrops is estimated by equation (5). Finally, the orographic rainfall is supposed to be a function of non-orographic rainfall and is calculated by solving the simultaneous equations (2) ~ (5) in multi-atmospheric layers.

$$R_{NWP} = R_o + R_n \quad (3)$$

$$R_o = \frac{L_{in} + WG\Delta t - L_{out}}{\Delta t} \times 3.6 \times H \quad (4)$$

$$c = 0.6778R_N^{0.731} \times 10^{-3} \quad (5)$$

where L_{in} and L_{out} are amounts of cloud water content (g/m^3) in an inflow and outflow side mesh, respectively. Δt is a timescale (s) during an air parcel passes one mesh, and H is the thickness of each layer (m).

Fig. 1 shows the procedure for the separation of

orographic and non-orographic rainfall. First, cloud water content is calculated from atmospheric variables of grid mesh in each layer vertically, and the ensemble NWP rainfall (R_{NWP}) is assumed to be that of the lowest layer (200 m height). It is separated into orographic (R_{o1}) and non-orographic (R_{n1}) rainfall by solving equations of (2) ~ (5). It is supposed that the non-orographic rainfall (R_{n1}) is expressed as the sum of the orographic rainfall (R_{o2}) and non-orographic rainfall (R_{n2}) in the upper layer. In this way, orographic rainfall and non-orographic rainfall of each layer can be separated from the lowest to the highest layer repeatedly. Then the non-orographic rainfall field of highest layer is utilized as an input domain for the transposition scheme to make additional ensemble information. And total orographic rainfall in each layer gives the value by recombining the transposition results of non-orographic rainfall field.

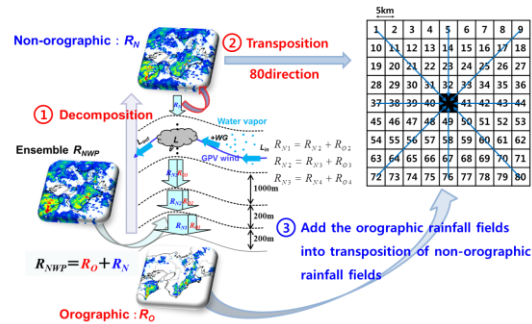


Fig. 1 The procedure of transposition method with consideration of orographic rainfall

2.2 Physically-based method for orographic rainfall

As previously stated, we examined the transposition scheme of non-orographic rainfall field in order to produce additional ensemble information and consider the misplacement from the original spatial position. Many EPSs are based on a Monte Carlo framework of NWP model with one realization starting from a central analysis (the control forecast) and others generated by perturbing the initial and/or boundary conditions (the perturbed forecasts) (Cloke and Pappenberger, 2009). In this study, we also used ensemble NWP rainfall created by perturbation of initial and boundary conditions, and we took into consideration the transposition scheme for more

additional ensembles. The technique for making additional ensemble information is fairly straightforward in this study. We utilized spatial transposition of each separated non-orographic rain fields.

Fig. 1 shows also a schematic of transposition scheme using non-orographic rainfall fields, and recombining with the total orographic rainfall in each vertical layer. For the transposition with separated non-orographic rainfall fields from the established ensemble prediction, the transposed catchment mask ($100\text{ km} \times 100\text{ km}$) moved into the original forecast domain from location 1 to 80 with a maximum distance in the x and y directions of each at about 20 km with 5 km interval in order to produce additional ensemble information. We finally constructed additional 891 transposed ensemble domains (existing 11 ensemble members \times 80 locations + 11 original locations of established ensemble members). Then final place-corrected ensemble rainfall fields are estimated by integrating the transposed non-orographic rain fields with the total orographic rainfall, which is calculated in each vertical layer.

3. DESIGN of METEOROLOGICAL EXPERIMENT

In Japan, the operational one-week ensemble prediction model from JMA was developed to provide probabilistic information of 51 ensemble members with a horizontal resolution of 60 km, and it used to be applied for hydrological applications (e.g., prior and optimized release discharge for dam operation; Matsubara et al., 2013). However, the operational short-term (1-2 days) ensemble prediction with much finer resolution has not been developed yet. For that reason, the ensemble forecast systems that are composed of 11 members (1 unperturbed and 10 perturbed member) with a horizontal resolution of 10 km and 2 km, the later nested inside the former with a 6-hour lag, has been experimentally conducted by the Meteorological Research Institute (MRI) of JMA for the 2011 typhoon Talas event.

Both 10 km and 2 km resolution systems used the JMA Non-Hydrostatic Model (NHM) as the forecast model (Saito et al., 2006; Saito, 2012).

Whereas the 10km resolution forecast adopted the cloud microphysical process and Kain-Fritsch convective scheme, the 2km resolution forecast did not use a convective scheme because of its cloud resolving resolutions. The domain of the two ensemble systems with 10 km and 2 km horizontal resolution are illustrated in Fig. 2.

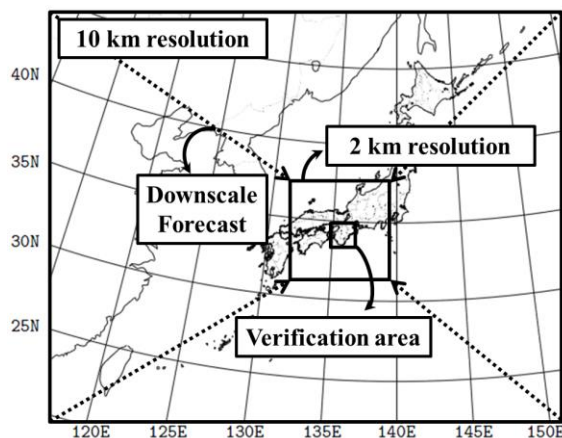


Fig. 2 Forecast domains of 10km and 2km horizontal resolution. The rectangle inside 2km domain denotes the verification area

The coarse resolution system of 10 km had a domain of 361×289 grid points with 50 vertical levels, forecasted up to 36 hours. For initial and lateral boundary conditions, 10 km used the analysis from the JMA non-hydrostatic 4DVAR (JNoVA) data assimilation system (Honda and Sawada, 2008) and the forecasts of JMA's high-resolution (TL959L60) global spectral model (GSM). The control run (cntl) is the forecast with a non-perturbed analysis, and the 10 perturbed forecasts were generated from JMA's 1-week global EPS (WEP) for the initial and boundary perturbations.

The fine resolution system of 2 km was conducted from downscale forecast of 10 km resolution systems. This system had a domain of 350×350 grid points with 60 vertical levels, and forecasted up to 30 hours. The initial and boundary condition for each member in 2 km were interpolated from the forecasts on the corresponding member in 10 km resolution with a 6-hour lag. 10 km started running at 21 JST every day, and 2 km with 6 hours later. Fig. 3 shows a schematic of forecast runs with 10 km and 2 km

resolution.

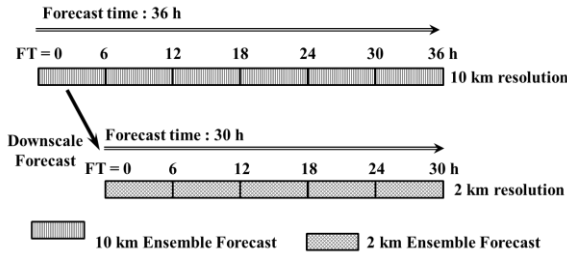


Fig. 3 Schematic of forecast runs with 10 km and 2 km horizontal resolution.

The ensemble prediction with a horizontal resolution of 2 km was performed with up to 30 h forecast time. In this study, the ensemble surface precipitation (Psr_f) from 2 km-downscaled NWP data with 30 h forecast time was utilized as input data into a hydrologic model.

4. A HYDROLOGICAL MODEL AND STUDY AREA

4.1 Distributed hydrologic model: KWMSS

In this study, we used a spatially-distributed hydrologic model, based on one-dimensional kinematic wave method for subsurface and surface flow (hereafter, KWMSS) with a conceptual stage-discharge relationship, which was introduced by Takasao and Shiiba (1988) and enhanced by Tachikawa et al. (2004).

In this model, the rainfall-runoff modeling system accepts spatially variable information in terms of topographic and meteorological data. The drainage network is represented by sets of hillslope and channel elements from digital elevation model (DEM). In this study, the drainage network was represented by a 250 m × 250 m spatial resolution of DEM. Fig. 5 is a conceptualization of spatial flow movement and flow process in hillslope elements of KWMSS. The rainfall over all hillslope elements flows one-dimensionally into the river nodes and then routes to the catchment outlet. The rainfall-runoff transformation conducted by KWMSS is based on the assumption that each hillslope element is covered with a permeable soil layer, as shown in Fig. 4. This soil layer consists of a capillary layer and a non-capillary layer. In these conceptual soil layers, slow and quick flow are

simulated as unsaturated Darcy flow and saturated Darcy flow, respectively, and overland flow occurs if water depth, h [m] exceeds soil water capacity.

$$q = \begin{cases} v_c d_c (h/d_c)^\beta, & 0 \leq h \leq d_c \\ v_c d_c + v_a (h - d_c), & d_c \leq h \leq d_s \\ v_c d_c + v_a (h - d_c) + \alpha (h - d_s)^m, & d_s \leq h \end{cases} \quad (6)$$

$$\frac{\partial h}{\partial t} + \frac{\partial q}{\partial x} = r(x, t) \quad (7)$$

where $v_c = k_c i$ [m/s], $v_a = k_a i$ [m/s], $k_c = k_a / \beta$ [m/s], $\alpha = i^{1/2} / n$ [m^{1/3}s⁻¹], $m = 5/3$, i is the slope gradient, k_c [m/s] is the hydraulic conductivity of the capillary soil layer, k_a [m/s] is the hydraulic conductivity of the non-capillary soil layer, n [m^{-1/3}] is the roughness coefficient, d_s [m] is the water depth corresponding to the water content, and d_c [m] is the water depth corresponding to maximum water content in the capillary pore.

The flow rate of each hillslope element q [m²/s] is calculated by equation (6), and combined with the continuity equation for channel routing by equation (7).

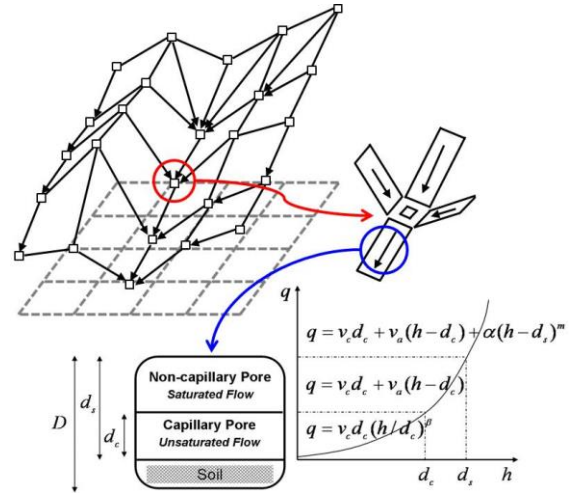


Fig. 4 Conceptualization of spatial flow movement and flow process in hillslope elements

4.2 Study area

The Shingu river basin was selected as the target area to compare flood forecast accuracy utilizing the original ensemble NWP rainfall with the results of transposition scheme of spatial rainfall fields as illustrated in Fig. 5(a). The Shingu river Basin is located in the Kii Peninsula of the Kinki area, Japan and covers an area of 2,360 km². The average elevation of the study site is 644.6 m,

and the slope is steep; this basin is a mountainous area. Fig. 5(b) shows the drainage network, which consists of channel and hillslope components of the Shingu river basin. The five dams, Futatsuno, Kazeya, Komori, Nanairo, and Ikehara are located upstream. Of the five dam catchments, we focused on two sub-catchments, which are Futatsuno (356.1 km²) and Nanairo (182.1 km²) dam catchments (Nos. 1 and 4 of Fig. 5(a)), to improve the accuracy of the flood forecasting in small catchments. Two additional dams, Kazeya and Ikehara (Nos. 2 and 5 of Fig. 5(a)), are located upstream of the Futatsuno and Nanairo catchments, respectively. Here, the observed outflows from the Kazeya and Ikehara dam were directly utilized as the upper boundary conditions for the subject dam basins to focus on only the Futatsuno and the Nanairo catchments. In this study, we assumed that evapotranspiration could be ignored during heavy rainfall event and directly used total rainfall for the rainfall–runoff simulation.

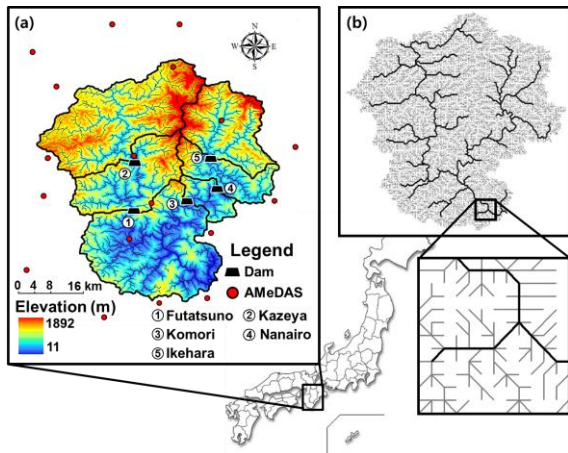


Fig. 5 (a) Shingu river basin, which is target area within Kii Peninsula in Japan and (b) drainage network represented by sets of channel (black line) and slope (gray line) elements.

5. RESULTS AND DISCUSSION

We applied the transposition scheme for non-orographic rainfall separated from ensemble NWP rainfall in order to produce more additional ensembles and investigate the misplaced spatial locations. As stated above, we finally constructed 891 transposed ensemble domains by integrating the transposed non-orographic rain fields with the

orographic rain fields.

Transposed ensemble domains have been verified spatially with MLIT observed radar rain data in the verification area to investigate the appropriate ensemble members and transposition locations, which have high efficiency criteria during rising limb of flood period (2011/9/2 3:00 ~ 9/3 9:00; 30 h forecast time with 30 min intervals) and applied them to the next peak discharge period of the flood forecasting (2011/09/03 3:00 ~ 09/04 9:00; 30h forecast time) for updating of flood forecasting. We used two popular indices to evaluate transposed ensemble domains: critical success index (CSI) for qualitative verification and root mean square error (RMSE) for quantitative verification, expressed as follows.

$$CSI = \frac{hits}{hits + misses + false\ alarms} \quad (8)$$

$$RMSE = \sqrt{\frac{1}{N} \sum_{t=1}^N (O_t - F_t)^2} \quad (9)$$

where N is the total grid cells (100×100) in verification area, O_t and F_t are the observed and forecasted rainfall of each grid cell at forecast time t , *hits* is the number of correct forecasts over the threshold (i.e., when the rainfall that is forecasted is also observed), and *misses* is the number of times rainfall is not forecasted, but is observed. *false alarms* is the number of times rainfall is forecasted, but not observed.

For the calculation of CSI value, the ensemble forecasts were expressed as probabilities of exceeding a selected rainfall threshold (10mm/h), which were used to compare an obvious spatial distribution of observed MLIT radar data with forecasted NWP rainfall. A contingency table can be constructed with a spatial comparison, in which each area with more than 10 mm/h of threshold is defined as "yes," and other areas are defined as "no" for both forecasted and observed rainfall fields.

Fig. 6 shows the results of the average CSI and RMSE of rising limb of flood period (2011/9/2 3:00 ~ 9/3 9:00; 30 h forecast time) in a comparison of observed radar rainfall and each transposed NWP rainfall domain. Each grid value means the average CSI and RMSE when a transposed mask domain

with the each grid as the center moved to an original domain with zero points of the x and y locations.

And we considered the top 10% transposition locations, which have high efficiency criteria for each RMSE and CSI value, of total 891 additional ensemble members in order to apply them to the next peak discharge period of the flood forecasting (2011/09/03 3:00 ~ 09/04 9:00; 30h forecast time), which we focused on in this study, to assess the accuracy improvement.

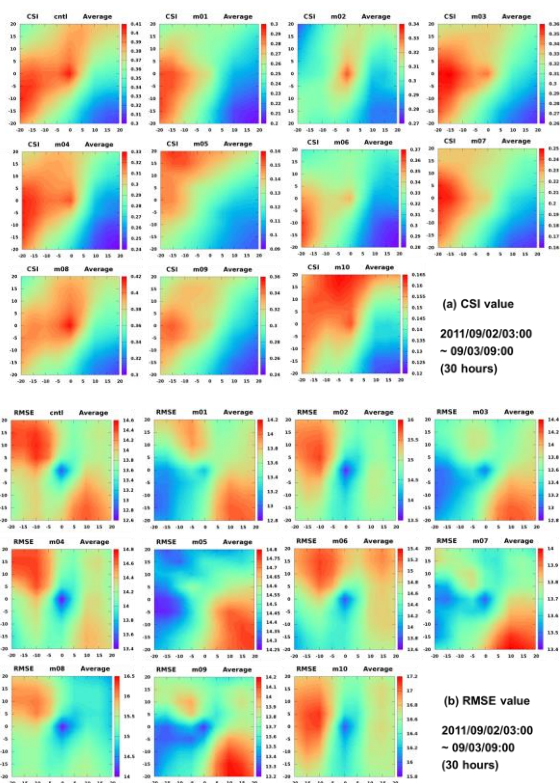


Fig. 6 Average CSI and RMSE results of rising limb of flood period (2011/9/2 3:00 ~ 9/3 9:00; 30 h forecast time) in a comparison of observed radar rainfall and each transposed

Base on the simulated results in the rising limb and peak discharge period, we compared the accuracy improvement with the results of the original ensemble flood forecasting for the former study using the mean absolute error (MAE), which is a quantity used to measure how close each forecast was to the observation.

Fig. 7 and 8 indicate the results of the 30 h ensemble flood forecast over the Futatsuno and Nanairo dam catchments during the rising limb and

peak discharge periods using the top 10% transposition locations of the ensemble rainfall fields. Table 1 compares the forecast skill of the original and transposition ensembles using the mean and best values of the flood forecasting.

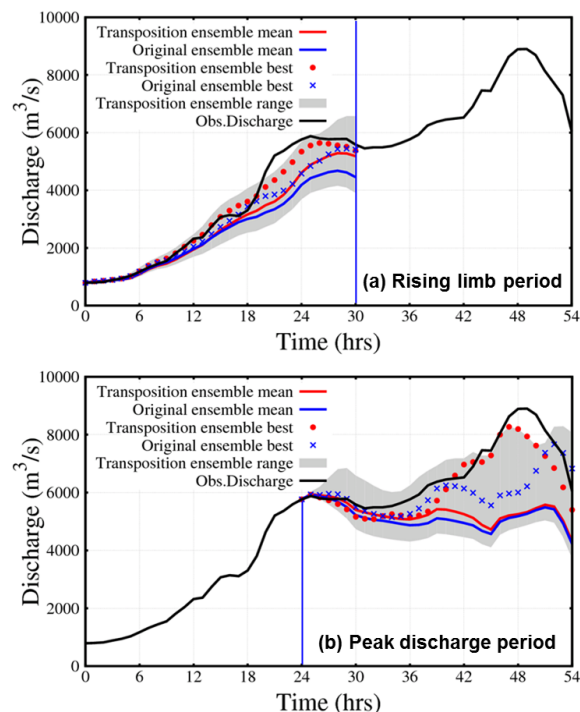


Fig. 7 30h ensemble flood forecasting using the transposition of ensemble rainfall fields during a rising limb period: (a) and (b) are the results of the rising limb and peak discharge period over the Futatsuno dam catchment.

Table 1 Comparisons of the original and transposition ensemble results in flood forecast skill: The bold red color indicates the better result, and members in parentheses refer to the member with the best flood forecast skill.

Catchment	Forecast Period	Type	MAE	
			Mean	Best
Futatsuno	Rising limb	Original	655.7	378.3 (m08)
		Transposition	469.2	196.0 (cntl_L6)
	Peak period	Original	1548.0	774.3 (m08)
		Transposition	1396.5	467.7 (m07_L38)
Nanairo	Rising limb	Original	270.8	206.2 (m03)
		Transposition	211.9	182.0 (m03_L39)
	Peak period	Original	1125.3	784.9 (m08)
		Transposition	1053.1	666.1 (m08_L37)

As shown in Fig. 4 and Table 3, the mean and best values during the peak discharge period for the Futatsuno dam catchment improved. The top 10% of transposition locations during the rising limb period and the transposition ensemble range were closer to the observed discharge than the original ensemble range. In the case of the Nanairo dam catchment (Table 1), the mean and best values also improved during the rising limb and peak discharge periods.

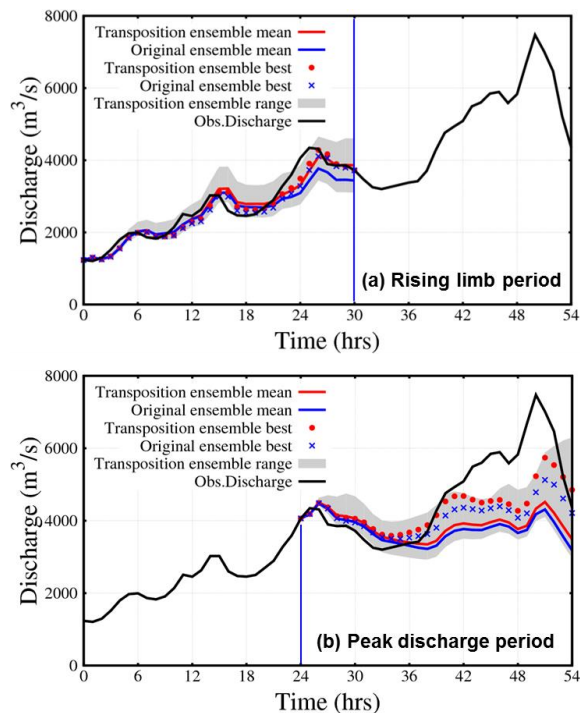


Fig. 8 30h ensemble flood forecasting using the transposition of ensemble rainfall fields during a rising limb period: (a) and (b) are the results of the rising limb and peak discharge period over the Nanairo dam catchment.

Based on these results, Addition ensemble members have the potential to provide the best value to flood forecasting skill when using the transposition method. Second, flood forecasting using the transposition of ensemble rainfall fields improved the accuracy for the under-predicted areas, and had better values than flood forecasting using the original ensemble members.

6. CONCLUSION

This study estimates the accuracy improvement of flood forecasting in the Futatsuno and the Nanairo dam catchments when driven by the transposition of ensemble NWP rainfall fields using the spatial verification of the RMSE and CSI values. The transposition locations for the rising limb period were adopted into flood forecasting for the peak discharge period to evaluate the improvement in accuracy. The ensemble flood forecasting using transposition of NWP rainfall fields produced better results than the original and selected ensemble members, in terms of the mean and best values of flood forecast skill in all periods over the two catchments.

In this study, we assessed the transposition method of ensemble NWP rainfall fields separately for the rising limb and peak discharge periods because they are the most important phases of real-time flood forecasting. However, it is very important to divide the periods, including the rising limb and peak discharge periods, when applying this method to an actual operation. Therefore, in further research, we need to consider the methodology required to divide the periods and to verify the applicability of these methods through a number of case studies. We expect it to be used in hydrological applications operationally, such as in real-time flood forecasting for warning systems and optimized release discharge for dam operations.

Acknowledgements

This study was partly supported by the sub-project of the field 3 on Next Generation Supercomputer Project, ‘Prediction of heavy rainfalls by a cloud-resolving NWP system’, and was based on data from J-POWER CO. Ltd. We are grateful for their support.

References

- Buizza, R., Miller, M., and Palmer, T. (1999) Stochastic representation of model uncertainties in the ECMWF Ensemble Prediction System, *Quart. J. Roy. Meteor. Soc.*, Vol.125, pp.2887–2908.

- Cloke, H.L. and Pappenberger, F. (2009) Ensemble flood forecasting: a review. *Journal of Hydrology*, Vol.375, pp.613-626.
- Cuo, L., Pagano, T.C. and Wang, Q.J. (2011) A review of quantitative precipitation forecasts and their use in short- to medium-range streamflow forecasting. *Journal of Hydrometeorology*, Vol.12, pp.713-728.
- Demeritt, D., Cloke, H., Pappenberger, F., Thielen, J., Bartholmes, J., and Ramos, M. (2007) Ensemble predictions and perceptions of risk, uncertainty, and error in flood forecasting. *Environ. Hazards*, Vol.7, pp.115–127.
- Ebert, E. and McBride, J. (2000) Verification of precipitation in weather systems: Determination of systematic errors. *Journal of Hydrology*, Vol.239, pp.179-202.
- Honda, Y. and Sawada, K. (2008) A new 4D-Var for mesoscale analysis at the Japan meteorological agency. *CAS/JSC WGNE Res. Act. Atmos. Ocea. Model*, Vol.38, pp.01.7-01.8.
- Matsubara, T., Kasahara, S., Shimada, Y., Nakakita, E., Tsuchida, K., and Takada, N. (2013) Study on applicability of information of typhoons and GSM for dam operation. *Ann. J. Hydraul. Eng. JSCE*, Vol.69, No.4, pp.367-372 (in Japanese with English abstract).
- Nakakita, E., Ikebuchi, S., Nakamura, T., Kanmuri, M., Okuda, M., Yamaji, A. and Takasao, T. (1996) Short-term rainfall prediction method using a volume scanning radar and GPV data from numerical weather prediction. *J. Geophys. Res.*, Vol.101, No.D21, pp.26181-26197.
- Nakakita, E. and Terazono, M. (2008) Short-term rainfall prediction taking into consideration nonlinear effect of non-orographic rainfall on orographic rainfall. *Ann. J. Hydraul. Eng. JSCE*, Vol.52, pp.331-336 (in Japanese with English abstract).
- Roulin, E. and Vannitsem, S. (2005) Skill of medium-range hydrological ensemble predictions. *Journal of Hydrometeorology*, Vol.6, No.5, pp.729-744.
- Saito, K., Fujita, T., Yamada, Y., Ishida, J., Kumagai, Y., Aranami, K., Ohmori, S., Nagasawa, R., Kumagai, S., Muroi, C., Kato, T., Eito, H. and Yamazaki, Y. (2006) The operational JMA nonhydrostatic meso-scale model. *Monthly Weather Review*, Vol.134, pp.1266-1298.
- Saito, K. (2012) The JMA nonhydrostatic model and its application to operation and research. In: Yucel, I. (Eds.), *Atmospheric Model Applications*, InTech, pp.85-110.
- Schaake, J., Perica, S., Mullusky, M., Demargne, J., Welles, E. and Wu, L. (2004) Pre-processing of atmospheric forcing for ensemble runoff prediction, *Proceedings of the 84th AMS Annual Meeting*.
- Tachikawa, Y., Nagatani, G. and Takara, K. (2004) Development of stage-discharge relationship equation incorporating saturated–unsaturated flow mechanism. *Ann. J. Hydraul. Eng. JSCE*, Vol.48, pp.7-12 (in Japanese with English abstract).
- Takasao, T. and Shiiba, M. (1988) Incorporation of the effect of concentration of flow into the kinematic wave equations and its applications to runoff system lumping. *Journal of Hydrology*, Vol.102, No.301-322.
- Tatehira, R. (1976) Orographic rainfall computation including cloud-precipitation interaction. *Tenki*, Vol.23, pp.95-100 (in Japanese).
- Xuan, Y., Cluckie, I. and Wang, Y. (2009) Uncertainty analysis of hydrological ensemble forecasts in a distributed model utilizing short-range rainfall prediction. *Hydrol. Earth Syst. Sci.*, Vol.13, pp.293-303.
- Yu, W., Nakakita, E. and Yamaguchi, K. (2013) Assessment of probabilistic flood Forecasting using ensemble NWP rainfall with 30hr forecast time during typhoon events. *Advances in River Engineering, JSCE*, Vol.19, pp.235-240.
- Yu, W., Nakakita, E., Kim, S. and Yamaguchi, K. (2013) Accuracy improvement of flood forecasting using pre-processing of ensemble numerical weather prediction rainfall fields. *Ann. J. Hydraul. Eng. JSCE*, Vol.70, No.4, pp.151-156.

(Received June 11, 2014)